
ENERGY BASED DIFFUSION GENERATOR FOR EFFICIENT SAMPLING OF BOLTZMANN DISTRIBUTIONS

Yan Wang^a, Ling Guo^b, Hao Wu^{c*}, Tao Zhou^d

^a School of Mathematical Sciences, Tongji University, Shanghai, P. R. China

^b Department of Mathematics, Shanghai Normal University, Shanghai, P. R. China

^c School of Mathematical Sciences, Institute of Natural Sciences and MOE-LSC, Shanghai Jiao Tong University, Shanghai, P. R. China

^d LSEC, Institute of Computational Mathematics and Scientific/Engineering Computing, AMSS, Chinese Academy of Sciences, Beijing, P. R. China

ABSTRACT

We introduce a novel sampler called the energy based diffusion generator for generating samples from arbitrary target distributions. The sampling model employs a structure similar to a variational autoencoder, utilizing a decoder to transform latent variables from a simple distribution into random variables approximating the target distribution, and we design an encoder based on the diffusion model. Leveraging the powerful modeling capacity of the diffusion model for complex distributions, we can obtain an accurate variational estimate of the Kullback-Leibler divergence between the distributions of the generated samples and the target. Moreover, we propose a decoder based on generalized Hamiltonian dynamics to further enhance sampling performance. Through empirical evaluation, we demonstrate the effectiveness of our method across various complex distribution functions, showcasing its superiority compared to existing methods.

1 INTRODUCTION

In various fields such as computational chemistry, statistical physics, and machine learning, the challenge of sampling from a Boltzmann distribution corresponding to a high-dimensional and complex energy function is ubiquitous. Unlike training tasks for data-driven generative models, where existing data can be leveraged to learn complex distributions, sampling from such Boltzmann distributions poses a distinct and formidable challenge due to the absence of readily available data. This presents a complex and difficult problem that has yet to be effectively addressed.

Markov Chain Monte Carlo (MCMC) methods have offered a pivotal solution to the challenge of sampling from high-dimensional distributions. These methods operate by iteratively generating candidates and updating samples, ultimately achieving asymptotic unbiasedness in the limit of infinite sampling steps (Hastings, 1970). To further amplify the sampling efficiency of MCMC, the integration of Brownian dynamics and Hamiltonian dynamics (Roberts & Tweedie, 1996; Neal et al., 2011; Betancourt et al., 2017; Cheng et al., 2018) has been introduced, providing a means to generate new samples. This integration results in improved acceptance probabilities and accelerated convergence rates. In recent years, researchers have proposed trainable transition kernels as a strategy for generating candidate samples, showcasing notable advancements in augmenting the efficiency and effectiveness of the sampling process (Song et al., 2017; Levy et al., 2017; Liu & Sun, 2022). However, the prolonged mixing time of MCMC still constrains its performance on high-dimensional complex distributions in practical applications.

Variational inference (VI) is another crucial approach for addressing intractable distributions. VI leverages a generator capable of swiftly producing samples to approximate the

*Corresponding Author, *Email address*: hwu81@sjtu.edu.cn (Hao Wu)

target Boltzmann distribution, and the optimization of the generator’s parameters is then undertaken to minimize a statistical distance, such as the Kullback-Leibler (KL) divergence, between the distribution of the generated samples and the target distribution. Due to its ability to model complex distributions and provide explicit probability density functions, normalizing flow (NF) has been extensively applied to construct generators for VI methods (Li & Wang, 2018; Noé et al., 2019; Köhler et al., 2020; Boyda et al., 2021; Vaitl et al., 2022; Albergo et al., 2022; Gerdes et al., 2022; Felardos, 2022; van Leeuwen et al., 2023; Plainer et al., 2023). However, the bijective nature of NFs imposes a constraint on their effective capacity, often rendering it insufficient for certain sampling tasks. When the probability density function of the generated sample distribution is unknown, leveraging Stein Discrepancy provides a means to construct the gradient flow of KL divergence for refining sample positions (Liu & Wang, 2016; Liu, 2017). However, these methods often involve computationally expensive tasks, requiring the computation of kernel functions and their gradients. In addition, the combination of MCMC and VI methods stands as a current focal point in research (Salimans et al., 2015; Zhang & Hernández-Lobato, 2018; Habib & Barber, 2018; Ruiz & Titsias, 2019; Wu et al., 2020; Shen et al., 2021). This combination seeks to harness the strengths of both approaches, offering a promising avenue for addressing the challenges associated with sampling from high-dimensional distributions and enhancing the efficiency of probabilistic modeling.

With the prosperity of diffusion based generative models (Sohl-Dickstein et al., 2015; Ho et al., 2020; Song et al., 2020; 2021), they have been applied to address challenges in the sampling problem. By training time-dependent score matching neural networks, methods proposed in (Zhang & Chen, 2021; Berner et al., 2022; Vargas et al., 2023) shape the Gaussian distribution into complex target densities, employing the KL divergence as the loss function. To mitigate mode-seeking issues, (Richter et al., 2023) introduces the log-variance loss, showcasing favorable properties. Additionally, an alternative training objective is outlined in (Máté & Fleuret, 2023), relying on flexible interpolations of the energy function and demonstrating substantial improvements for multi-modal targets. However, a common drawback of these methods is their dependence on numerical differential equation solvers to compute time integrals, which can incur both significant computational costs and time constraints.

In this research endeavor, we present a novel approach termed the energy based diffusion generator (EDG), drawing inspiration from both VI techniques and the diffusion model. The architecture of EDG closely resembles that of a variational autoencoder (VAE) (Kingma et al., 2019), comprising a decoder and an encoder. The decoder is flexible in mapping latent variables distributed according to tractable distributions to samples, without the imposition of constraints such as bijectivity, and we design in this work a decoder based on generalized Hamiltonian dynamics to enhance sampling efficiency. The encoder utilizes a diffusion process, enabling the application of score matching techniques for precise and efficient modeling of the conditional distribution of latent variables given samples. Unlike existing diffusion based methods, the loss function of EDG allows for the convenient computation of unbiased estimates in a mini-batch fashion, eliminating the need for numerical solutions to ordinary differential equations (ODEs) or stochastic differential equations (SDEs) during training. Numerical experiments conclusively demonstrate the effectiveness of EDG.

2 PRELIMINARIES AND SETUP

In this work, we delve into the task of crafting generative models for the purpose of sampling from the Boltzmann distribution driven by a predefined energy $U : \mathbb{R}^d \rightarrow \mathbb{R}$:

$$\pi(x) = \frac{1}{Z} \exp(-U(x)),$$

where the normalizing constant $Z = \int \exp(-U(x))dx$ is usually computationally intractable. To tackle this challenge, the Boltzmann generator (Noé et al., 2019), along with its various extensions (Felardos, 2022; van Leeuwen et al., 2023; Plainer et al., 2023), has emerged as a prominent technique in recent years. These approaches harness NF to parameterize a trainable and analytical density function, with parameter optimization achieved through the

minimization of the KL divergence between the surrogate density and π . Nevertheless, in contrast to typical generative models, the pursuit of exact probability density computation imposes substantial constraints on NFs: Each transformation layer must be a bijection, and the determinant of its Jacobian matrix can be tractably computed. These requirements inherently limit the capacity of NFs to effectively model complex distributions.

Our focus now shifts to a generator akin to the VAE. This generator produces samples by a decoder as

$$x|z_0 \sim p_D(x|z_0, \phi),$$

Here, $z_0 \sim p_D(z_0)$ is a tractable latent variable with a known prior distribution, often a standard multivariate normal distribution, and ϕ denotes the parameter of the decoder. Similar to the VAE, we can formulate $p_D(x|z_0; \phi)$ as $\mathcal{N}(x|\mu(z_0; \phi), \Sigma(z_0; \phi))$, where both μ and Σ are represented by neural networks (NNs).

While the marginal distribution $p_D(x)$ of generator samples remains intractable, we can derive an upper bound for the KL divergence:

$$\begin{aligned} D_{KL}(p_D(x)||\pi(x)) &\leq D_{KL}(p_D(z_0) \cdot p_D(x|z_0, \phi)||\pi(x) \cdot p_E(z_0|x, \theta)) \\ &= \mathbb{E}_{p_D(z_0) \cdot p_D(x|z_0, \phi)} \left[\log \frac{p_D(z_0)p_D(x|z_0, \phi)}{p_E(z_0|x, \theta)} + U(x) \right] + \log Z. \quad (1) \end{aligned}$$

Here, the parametric distribution $p_E(z_0|x, \theta)$ defines an encoder that maps from x to the latent variable z , and the equality is achieved if $p_E(z|x, \theta)$ matches the conditional distribution of z for a given x , deduced from the decoder.

It seems that we have only increased the complexity of the problem, as we are still required to approximate a conditional distribution. However, in the upcoming section, we demonstrate that we can effectively construct the encoder using the diffusion model (Sohl-Dickstein et al., 2015; Song et al., 2020) and optimize all parameters without the need to numerically solve ordinary or stochastic differential equations.

3 ENERGY BASED DIFFUSION GENERATOR

Motivated by the diffusion model (Song et al., 2020; 2021), we now discuss the idea of the energy based diffusion generator (EDG). In the EDG framework, we initiate a diffusion process from the latent variable z_0 and combine it with the decoder, resulting in what we term the “decoding process”:

$$\begin{aligned} z_0 \in R^D \sim p_D(z_0), \quad x|z_0 \sim p_D(x|z_0; \phi) \\ dz_t = f(z_t, t)dt + g(t)dW_t, \quad t \in [0, T] \end{aligned} \quad (2)$$

where W_t is the standard Wiener process, $f(\cdot, t) : R^D \rightarrow R^D$ acts as the drift coefficient, and $g(\cdot) : R \rightarrow R$ serves as the diffusion coefficient. To streamline notation, we denote the probability distribution defined by the decoding process as p_D . In typical SDEs applied in diffusion models, two critical conditions hold: (a) the transition density $p_D(z_t|z_0)$ can be analytically computed without numerically solving the Fokker-Planck equation, and (b) z_T is approximately uninformative with $p_D(z_T) \approx p_D(z_T|z_0)$.

Now, let’s explore a scenario where the initial distribution of z_0 in (2) is defined as $p_D(z_0|x) \propto p_D(z_0) \cdot p_D(x|z_0)$. In this context, we can derive the following reverse-time diffusion equation (Anderson, 1982):

$$dz_{\tilde{t}} = - (f(z_{\tilde{t}}, \tilde{t}) - g(\tilde{t})^2 \nabla_{z_{\tilde{t}}} \log p_D(z_{\tilde{t}}|x)) d\tilde{t} + g(\tilde{t})dW_{\tilde{t}}, \quad (3)$$

where $\tilde{t} = T - t$ denotes the reverse time. Since the independence between z_T and z_0 also implies the independence between z_T and x , we can simulate (3) by initializing it from the marginal distribution of $p_D(z_T)$ to acquire samples of $p_D(z_0|x)$. Nonetheless, practical implementation of this simulation presents challenges due to the intractability of the score function $\nabla_{z_{\tilde{t}}} \log p_D(z_{\tilde{t}}|x)$. To address this challenge, we resort to approximating the score function using a parametric model denoted as $s(z_{\tilde{t}}, x, \tilde{t}; \theta)$. This approximation leads to what

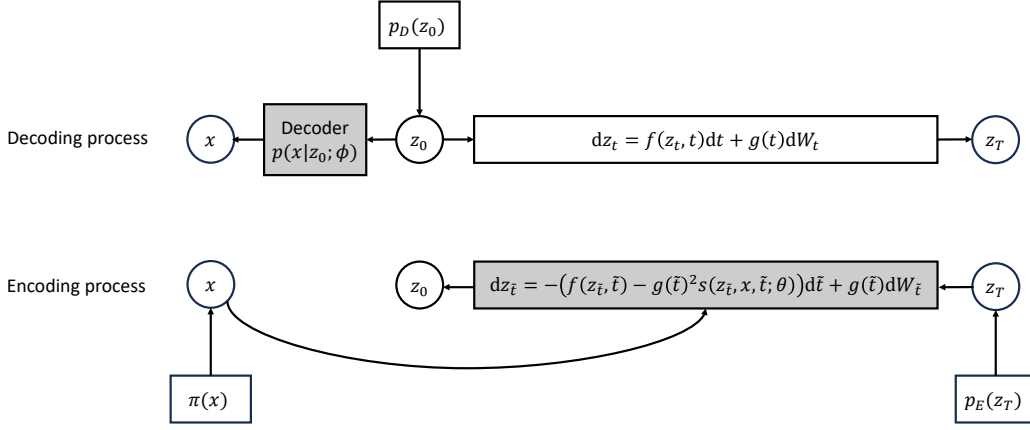


Figure 1: Probabilistic graphs of the decoding and encoding processes, highlighting the trainable parts of the model in gray.

we refer to as the “encoding process”, achieved by integrating the parametric reverse-time diffusion process and the target distribution of x :

$$\begin{aligned} x &\sim \pi(x), \quad z_T \sim p_E(z_T) \triangleq p_D(z_T) \\ dz_{\tilde{t}} &= -(f(z_{\tilde{t}}, \tilde{t}) - g(\tilde{t})^2 s(z_{\tilde{t}}, x, \tilde{t}; \theta))d\tilde{t} + g(\tilde{t})dW_{\tilde{t}}, \quad \tilde{t} = T - t. \end{aligned} \quad (4)$$

For simplicity of notation, we refer to the distribution defined by the encoding process as p_E in this paper.

Fig. 1 offers a visual depiction of the decoding and encoding processes.

3.1 LOSS FUNCTION

To optimize parameters of the decoding and encoding processes, we can minimize the KL divergence between the joint distributions of $(x, z_{[\cdot]})$ provided by the decoding and encoding processes, where $z_{[\cdot]}$ denotes the path $\{z_t\}_{t \in [0, T]}$ from 0 to T . The divergence is also an upper bound of $D_{KL}(p_E(x) || \pi(x))$ like that in (1) due to the data processing inequality, and can be expressed as

$$D_{KL}(p_D(x, z_{[\cdot]}) || p_E(x, z_{[\cdot]})) = \mathcal{L}(\theta, \phi) + \log Z, \quad (5)$$

where

$$\begin{aligned} \mathcal{L}(\theta, \phi) &= \mathbb{E}_{p_D} [\log p_D(x|z_0; \phi) + U(x)] \\ &+ \int_0^T \frac{g(t)^2}{2} \mathbb{E}_{p_D} \left[\|s(z_t, x, t; \theta)\|^2 + 2\nabla_{z_t} \cdot s(z_t, x, t; \theta) + \|\nabla_{z_t} \log p_D(z_t)\|^2 \right] dt. \end{aligned} \quad (6)$$

By utilizing the importance-sampled integration and Hutchinson estimator, we can obtain an equivalent expression of $\mathcal{L}(\theta, \phi)$ which can be efficiently and unbiasedly estimated by a small batch of samples of p_D :

$$\begin{aligned} \mathcal{L}(\theta, \phi) &= \mathbb{E}_{p_D} [\log p_D(x|z_0; \phi) + U(x)] \\ &+ \int_0^T \lambda(t) \cdot \mathbb{E}_{p(t)p(\epsilon)p_D(x, z_t)} [\mathcal{L}_t(x, z_t, \epsilon; \theta)] dt, \end{aligned} \quad (7)$$

where

$$\mathcal{L}_t(x, z_t, \epsilon; \theta) = \|s(z_t, x, t; \theta)\|^2 + 2 \frac{\partial [\epsilon^\top s(z_t, x, t; \theta)]}{\partial z_t} \epsilon + \|\nabla_{z_t} \log p_D(z_t)\|^2,$$

$p(\epsilon)$ is the Rademacher distribution with $\mathbb{E}[\epsilon] = 0$, $\text{cov}(\epsilon) = I$, $p(t)$ is a proposal distribution of $t \in [0, T]$, and the weighting function $\lambda(t) = \frac{g(t)^2}{2p(t)}$.

The selection of $p(t)$ significantly influences the stochastic approximation of the second term on the r.h.s of (7). To mitigate the variance inherent in this approximation, we adopt a strategic approach outlined in (Choi et al., 2022), wherein we dynamically adjust the proposal distribution based on the historical buffer encompassing the B most recent loss values concerning t within the second term of (7).

For a comprehensive understanding of the loss function and the update strategy for $p(t)$, please refer to Appendix C, where detailed derivations are provided.

3.2 BOUNDARY CONDITION-GUIDED ENCODER FORMULATION

Considering that the true score function satisfies the following boundary conditions for $t = 0, T$:

$$\begin{aligned} \nabla_{z_0} \log p_D(z_0|x) &= \nabla_{z_0} [\log p_D(z_0|x) + \log p_D(x)] \\ &= \nabla_{z_0} \log p_D(x, z_0) \\ &= \nabla_{z_0} [\log p_D(x|z_0) + \log p_D(z_0)] \end{aligned}$$

and

$$\nabla_{z_T} \log p_D(z_T|x) = \nabla_{z_T} \log p_D(z_T),$$

we propose to express $s(z, x, t; \theta)$ as

$$\begin{aligned} s(z, x, t; \theta) &= \left(1 - \frac{t}{T}\right) \cdot \nabla_{z_0} [\log p_D(x|z_0 = z) + \log p_D(z_0 = z)] + \frac{t}{T} \cdot \nabla_{z_T} \log p_D(z_T = z) \\ &\quad + \frac{t}{T} \left(1 - \frac{t}{T}\right) s'(z, x, t; \theta), \end{aligned}$$

where $s'(z, x, t; \theta)$ is the neural network to be trained. This formulation ensures that the error of s is zero for both $t = 0$ and $t = T$.

3.3 COMPUTATION OF MARGINAL ENCODER DENSITY

In line with the proof detailed in Appendix D of (Song et al., 2020), we can assert that the temporal evolution of $p_E(z_t|x)$ within the reverse-time diffusion process (4) adheres to the probability flow ordinary differential equation (ODE):

$$\begin{aligned} dz_t &= \left(f(z_t, t) - \frac{1}{2} g(t)^2 s(z_t, x, t|\theta) \right) dt \\ &\triangleq f^{PF}(z_t, x, t|\theta) dt \end{aligned} \tag{8}$$

This alignment holds true if $s(z_t, x, t|\theta)$ effectively approximates the score function $\nabla_{z_t} \log p_E(z_t|x)$ after training.

As a consequence, given x and z_0 , we can numerically solve the ODE to trace the path z_t^{PF} , initiated with $z_0^{PF} = z_0$. The computation of the marginal encoder density $p_E(z_0|x)$ adheres to the principles of neural ODE (Chen et al., 2018), expressed as:

$$\log p_E(z_0|x) = \log p_E(z_T^{PF}) + \int_0^T \text{tr} \left(\frac{\partial f^{PF}(z_t^{PF}, x, t|\theta)}{\partial z_t^{PF}} \right) dt. \tag{9}$$

Based on the aforementioned findings, we can efficiently estimate the normalizing constant Z and utilize importance sampling techniques to further correct modeling errors in EDG. (See Appendix B.)

3.4 DECODING WITH GENERALIZED HAMILTONIAN DYNAMICS

In our investigation, we observed that EDG performs poorly for multimodal distributions, primarily due to the mode-seeking behavior of the KL divergence. To address this limitation, we propose a decoder based on generalized Hamiltonian dynamics (GHD) (Song et al., 2017; Levy et al., 2017), summarized in Algorithm 1, which significantly enhances the sampling performance for multimodal distributions.

Within the algorithm, we initially stochastically generate a sample y using the random variable ζ (refer to Line 1 of the algorithm). Subsequently, we iteratively update the sample using random velocities v_1, \dots, v_K and Generalized Hamiltonian Dynamics (see Line 5). Finally, we utilize discretized Brownian dynamics with a trainable step size to design the decoder density of x (refer to Line 9). Notably, the parameters of A , T_v , Q_v , ϵ , and η are all trainable, and ϵ_0 serves as a hyperparameter. Our numerical experiments suggest that setting ϵ_0 to a small positive value can improve the stability of the algorithm.

Algorithm 1 GHD based decoder

Require: $z_0 = (\zeta, v_1, \dots, v_K)$ drawn from the standard Gaussian distribution and decoder parameters ϕ

```

1: Let  $y := a(\zeta; \phi)$ .
2: for  $k = 1, \dots, K$  do
3:   for  $j = 1, \dots, J$  do
4:     Let  $s := \frac{(k-1)J+j-1}{KJ}$ .
5:     Update  $(y, v_i)$  by
        
$$v_k := v_k - \frac{\epsilon(s; \phi)}{2} \left( \nabla U(y) \odot e^{\frac{\epsilon_0}{2} Q_v(y, \nabla U(y), s; \phi)} + T_v(y, \nabla U(y), s; \phi) \right)$$

        
$$y := y + \epsilon(s; \phi) \left( v_k \odot e^{\epsilon_0 Q_y(v_k, s; \phi)} + T_y(v_k, s; \phi) \right)$$

        
$$v_k := v_k - \frac{\epsilon(s; \phi)}{2} \left( \nabla U(y) \odot e^{\frac{\epsilon_0}{2} Q_v(y, \nabla U(y), s; \phi)} + T_v(y, \nabla U(y), s; \phi) \right)$$

6:   end for
7:   Let  $v_k := -v_k$ .
8: end for
9: Let  $\mu = y - e^{\epsilon_0 \eta(y; \phi)} \nabla U(y)$  and  $\Sigma = 2e^{\epsilon_0 \eta(y; \phi)} I$ .
10: return  $x \sim \mathcal{N}(\mu, \Sigma)$ .
```

In the experiments of this paper, unless explicitly stated otherwise, EDG will utilize a GHD based decoder.

4 EXPERIMENTS

We empirically evaluate EDG across a diverse range of energy functions. Initially, we present the results obtained from a set of two-dimensional distributions. Subsequently, we demonstrate the performance of EDG in the context of Bayesian logistic regression. All the experimental details are provided in Appendix D.

2D energy function Firstly, we compare our model with HMC (Neal et al., 2011), VAE and BG (Noé et al., 2019) on several synthetic 2D energy functions: MoG2(i) (Mixture of two isotropic Gaussians with the same $\sigma^2 = 0.5$ or different variance $\sigma_1^2 = 1.5, \sigma_2^2 = 0.3$ and centroids separated by distance 10), MoG6 (Mixture of six isotropic Gaussians with variance $\sigma^2 = 0.1$), MoG9 (Mixture of nine isotropic Gaussians with variance $\sigma^2 = 0.3$) Ring, Ring5. For HMC, we conducted 500 independent runs, each providing 1,000 samples after a burn-in phase of 1,000 steps. The VAE architecture closely mirrors that of EDG, utilizing the loss defined in (1). Here, the decoder incorporates a prior distribution for z_0 denoted by $p_D(z_0) \sim \mathcal{N}(0, I)$, and both $p_D(x|z_0)$ and $p_E(z_0|x)$ are modeled as Gaussian distributions. Additionally, multilayer perceptrons (MLPs) are employed to compute the

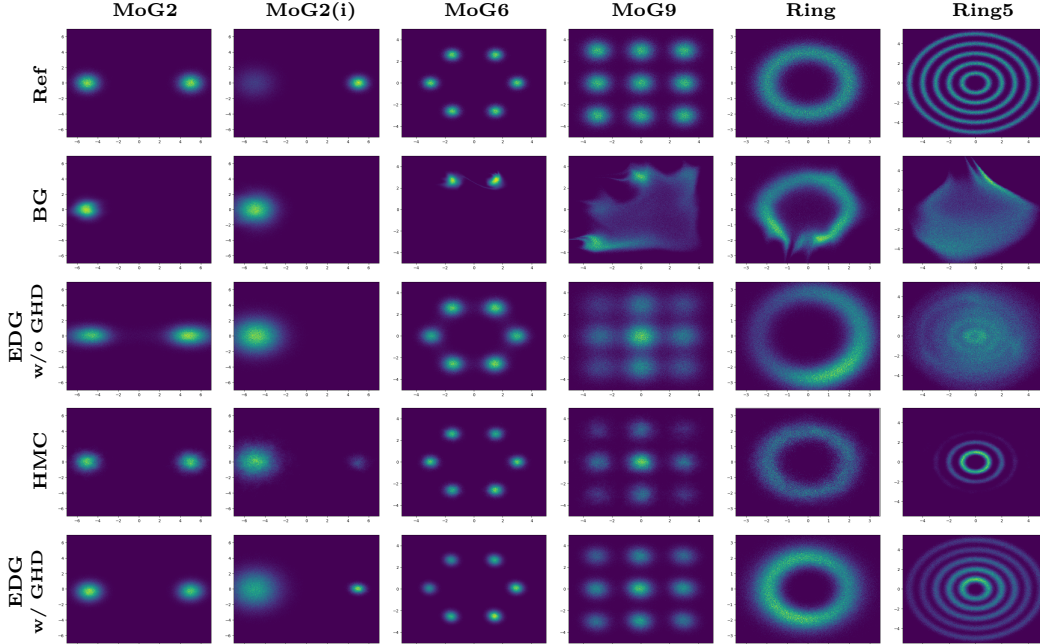


Figure 2: Density plots for 2D energy function. For the generation of reference samples, please refer to Appendix D. We generate 500,000 samples for each method and plot the histogram.

The Maximum Mean Discrepancy (MMD) of 2D energy tasks.							
	Mog2	Mog2(i)	Mog6	Mog9	Ring	Ring5	
VAE	1.86	1.62	2.57	0.17	0.11	0.36	
BG	1.90	1.63	2.64	0.07	0.05	0.18	
HMC	0.01	1.56	0.02	0.04	0.01	0.82	
EDG w/o GHD	0.06	1.30	0.04	0.05	0.09	0.05	
EDG w/ GHD	0.01	1.14	0.01	0.02	0.01	0.03	

Table 1: The maximum mean discrepancy between the samples generated by each generator and the reference samples. Details on the calculation of discrepancy can be found in Appendix D.

means and variances of $p_D(x|z_0)$ and $p_E(z_0|x)$. The BG employs RealNVP, comprising 6 affine coupling layers, where the scaling and shifting operations for each layer are executed by MLPs with two hidden layers, and each layer of MLPs consists of 256 hidden units. We draw the histogram of samples for visual inspection in Fig. 2. In addition, for EDG, we also compared the sampling performance between a GHD based decoder (EDG w/ GHD) and a conventional decoder (EDG w/o GHD). The sampling results are summarized in Fig. 2 and Table 1. It can be seen that the EDG with GHD based decoder outperforms other methods.

Bayesian Logistic Regression In the subsequent experiments, we highlight the efficacy of EDG in the context of Bayesian logistic regression, particularly when dealing with a posterior distribution residing in a higher-dimensional space. In this scenario, we tackle a binary classification problem with labels $L = \{0, 1\}$ and high-dimensional features D . The classifier’s output is defined as

$$p(L = 1|D, x) = \text{softmax}(w^\top D + b),$$

	AU		GE		HE	
	Acc	Auc	Acc	Auc	Acc	Auc
HMC	82.97 ± 1.94	90.88 ± 0.83	78.52 ± 0.48	77.67 ± 0.28	86.75 ± 1.63	93.35 ± 0.76
VAE	82.84 ± 1.06	91.16 ± 0.37	78.22 ± 1.27	77.74 ± 1.14	86.81 ± 2.66	93.33 ± 1.16
BG	82.99 ± 1.18	91.23 ± 0.67	78.14 ± 1.44	77.59 ± 0.73	86.75 ± 1.99	93.44 ± 0.39
EDG	83.15 ± 1.01	91.63 ± 0.47	78.94 ± 0.92	78.11 ± 0.70	87.56 ± 2.23	94.35 ± 0.76

Table 2: Classification accuracy and AUC results for Bayesian logistic regression tasks. The experiments utilize consistent training and test data partitions, where the HMC step size is set to 0.01, and EDG utilizes the GHD based decoder. Average accuracy and AUC values, accompanied by their respective standard deviations, are computed across 32 independent experiments for all datasets.

	HMC	VAE	BG	EDG
Acc	49.88 ± 3.32	50.99 ± 2.67	50.75 ± 3.78	70.13 ± 2.13

Table 3: Classification accuracy on the test dataset of Coverstype. The reported values represent averages and standard deviations of accuracy over 32 independent experiments. The GHD based decoder is used in EDG.

where $x = (w, b)$. Drawing samples x^1, \dots, x^N from the posterior distribution

$$\pi(x) \propto p(x) \prod_{(L,D) \in \mathcal{D}_{\text{train}}} p(L|D, x)$$

based on the training set $\mathcal{D}_{\text{train}}$, where the prior distribution $p(x)$ is a standard Gaussian distribution. For L, D in the test dataset, $p(L|D, \mathcal{D}_{\text{train}})$ is approximated as $\sum_n p(L|D, x^n)$. We conduct experiments on three datasets: Australian (AU, 15 covariates), German (GE, 25 covariates), and Heart (HE, 14 covariates) (Dua & Graff, 2017), evaluating accuracy rate (ACC) and Area Under the Curve (AUC) on the test subset. Remarkably, as illustrated in Table 2, EDG consistently achieves the highest accuracy and AUC performance.

We extend our analysis to the binary Covertype dataset comprising 581,012 data points and 54 features. The posterior of the classifier parameters follows a hierarchical Bayesian model (matching the model in Section 5 of (Liu & Wang, 2016)), with x denoting the combination of classifier parameters and the hyperparameter in the hierarchical Bayesian model. To enhance computational efficiency, in VAE, BG, and EDG, $\log \pi(x)$ is unbiasedly approximated during training as

$$\log \pi(x) \approx \log p(x) + \frac{|\mathcal{D}_{\text{train}}|}{|\mathcal{B}|} \sum_{(L,D) \in \mathcal{B}} \log p(L|D, x),$$

where \mathcal{B} is a random mini-batch. For HMC, the exact posterior density is calculated. As indicated by the results in Table 3, EDG consistently outperforms alternative methods.

5 CONCLUSION

In summary, our work introduces the EDG as an innovative and effective sampling approach by combining principles from VI and diffusion based methods. Drawing inspiration from VAEs, EDG excels in efficiently generating samples from intricate Boltzmann distributions. Leveraging the expressive power of the diffusion model, our method accurately estimates the KL divergence without the need for numerical solutions to ordinary or stochastic differential equations. Empirical experiments validate the superior sampling performance of EDG.

Looking forward, our primary focus will be on extending the application of EDG to construct generative models for large-scale physical and chemical systems, such as proteins (Zheng et al., 2023; Jing et al., 2023).

REFERENCES

- Michael S Albergo, Denis Boyda, Kyle Cranmer, Daniel C Hackett, Gurtej Kanwar, Sébastien Racanière, Danilo J Rezende, Fernando Romero-López, Phiala E Shanahan, and Julian M Urban. Flow-based sampling in the lattice schwinger model at criticality. *Physical Review D*, 106(1):014514, 2022.
- Brian DO Anderson. Reverse-time diffusion equation models. *Stochastic Processes and their Applications*, 12(3):313–326, 1982.
- Julius Berner, Lorenz Richter, and Karen Ullrich. An optimal control perspective on diffusion-based generative modeling. *arXiv preprint arXiv:2211.01364*, 2022.
- Michael Betancourt, Simon Byrne, Sam Livingstone, and Mark Girolami. The geometric foundations of hamiltonian monte carlo. *Bernoulli*, 23(4A):2257–2298, 2017.
- Denis Boyda, Gurtej Kanwar, Sébastien Racanière, Danilo Jimenez Rezende, Michael S Albergo, Kyle Cranmer, Daniel C Hackett, and Phiala E Shanahan. Sampling using su (n) gauge equivariant flows. *Physical Review D*, 103(7):074504, 2021.
- Ricky TQ Chen, Yulia Rubanova, Jesse Bettencourt, and David K Duvenaud. Neural ordinary differential equations. *Advances in neural information processing systems*, 31, 2018.
- Xiang Cheng, Niladri S Chatterji, Peter L Bartlett, and Michael I Jordan. Underdamped langevin mcmc: A non-asymptotic analysis. In *Conference on learning theory*, pp. 300–323. PMLR, 2018.
- Kristy Choi, Chenlin Meng, Yang Song, and Stefano Ermon. Density ratio estimation via infinitesimal classification. In *International Conference on Artificial Intelligence and Statistics*, pp. 2552–2573. PMLR, 2022.
- Laurent Dinh, Jascha Sohl-Dickstein, and Samy Bengio. Density estimation using real nvp. *arXiv preprint arXiv:1605.08803*, 2016.
- D. Dua and C. Graff. Uci machine learning repository. <https://archive.ics.uci.edu/ml/index.php>, 2017. Accessed: 2022-03-13.
- Loris Felardos. *Data-free Generation of Molecular Configurations with Normalizing Flows*. PhD thesis, Université Grenoble Alpes, 2022.
- Mathis Gerdes, Pim de Haan, Corrado Rainone, Roberto Bondesan, and Miranda CN Cheng. Learning lattice quantum field theories with equivariant continuous flows. *arXiv preprint arXiv:2207.00283*, 2022.
- Arthur Gretton, Karsten M Borgwardt, Malte J Rasch, Bernhard Schölkopf, and Alexander Smola. A kernel two-sample test. *The Journal of Machine Learning Research*, 13(1): 723–773, 2012.
- Raza Habib and David Barber. Auxiliary variational mcmc. In *International Conference on Learning Representations*, 2018.
- W Keith Hastings. Monte carlo sampling methods using markov chains and their applications. *Biometrika*, 1970.
- Jonathan Ho, Ajay Jain, and Pieter Abbeel. Denoising diffusion probabilistic models. *Advances in neural information processing systems*, 33:6840–6851, 2020.
- Bowen Jing, Ezra Erives, Peter Pao-Huang, Gabriele Corso, Bonnie Berger, and Tommi Jaakkola. Eigenfold: Generative protein structure prediction with diffusion models. *arXiv preprint arXiv:2304.02198*, 2023.
- Diederik P Kingma, Max Welling, et al. An introduction to variational autoencoders. *Foundations and Trends® in Machine Learning*, 12(4):307–392, 2019.

-
- Jonas Köhler, Leon Klein, and Frank Noé. Equivariant flows: exact likelihood generative learning for symmetric densities. In *International conference on machine learning*, pp. 5361–5370. PMLR, 2020.
- Daniel Levy, Matthew D Hoffman, and Jascha Sohl-Dickstein. Generalizing hamiltonian monte carlo with neural networks. *arXiv preprint arXiv:1711.09268*, 2017.
- Shuo-Hui Li and Lei Wang. Neural network renormalization group. *Physical review letters*, 121(26):260601, 2018.
- Qiang Liu. Stein variational gradient descent as gradient flow. *Advances in neural information processing systems*, 30, 2017.
- Qiang Liu and Dilin Wang. Stein variational gradient descent: A general purpose bayesian inference algorithm. *Advances in neural information processing systems*, 29, 2016.
- Shaofan Liu and Shiliang Sun. Adversarially training mcmc with non-volume-preserving flows. *Entropy*, 24(3):415, 2022.
- Bálint Máté and François Fleuret. Learning interpolations between boltzmann densities. *Transactions on Machine Learning Research*, 2023.
- Radford M Neal et al. Mcmc using hamiltonian dynamics. *Handbook of markov chain monte carlo*, 2(11):2, 2011.
- Frank Noé, Simon Olsson, Jonas Köhler, and Hao Wu. Boltzmann generators: Sampling equilibrium states of many-body systems with deep learning. *Science*, 365(6457): eaaw1147, 2019.
- Michael Plainer, Hannes Stark, Charlotte Bunne, and Stephan Günnemann. Transition path sampling with boltzmann generator-based mcmc moves. In *NeurIPS 2023 AI for Science Workshop*, 2023.
- Lorenz Richter, Julius Berner, and Guan-Horng Liu. Improved sampling via learned diffusions. *arXiv preprint arXiv:2307.01198*, 2023.
- Gareth O Roberts and Richard L Tweedie. Exponential convergence of langevin distributions and their discrete approximations. *Bernoulli*, pp. 341–363, 1996.
- Francisco Ruiz and Michalis Titsias. A contrastive divergence for combining variational inference and mcmc. In *International Conference on Machine Learning*, pp. 5537–5545. PMLR, 2019.
- Tim Salimans, Diederik Kingma, and Max Welling. Markov chain monte carlo and variational inference: Bridging the gap. In *International conference on machine learning*, pp. 1218–1226. PMLR, 2015.
- Zheyang Shen, Markus Heinonen, and Samuel Kaski. De-randomizing mcmc dynamics with the diffusion stein operator. *Advances in Neural Information Processing Systems*, 34: 17507–17517, 2021.
- Jascha Sohl-Dickstein, Eric Weiss, Niru Maheswaranathan, and Surya Ganguli. Deep unsupervised learning using nonequilibrium thermodynamics. In *International conference on machine learning*, pp. 2256–2265. PMLR, 2015.
- Jiaming Song, Shengjia Zhao, and Stefano Ermon. A-nice-mc: Adversarial training for mcmc. *Advances in Neural Information Processing Systems*, 30, 2017.
- Yang Song, Jascha Sohl-Dickstein, Diederik P Kingma, Abhishek Kumar, Stefano Ermon, and Ben Poole. Score-based generative modeling through stochastic differential equations. *arXiv preprint arXiv:2011.13456*, 2020.
- Yang Song, Conor Durkan, Iain Murray, and Stefano Ermon. Maximum likelihood training of score-based diffusion models. *Advances in Neural Information Processing Systems*, 34: 1415–1428, 2021.

-
- Lorenz Vaitl, Kim A Nicoli, Shinichi Nakajima, and Pan Kessel. Gradients should stay on path: better estimators of the reverse-and forward kl divergence for normalizing flows. *Machine Learning: Science and Technology*, 3(4):045006, 2022.
- Steyn van Leeuwen, Alberto Pérez de Alba Ortíz, and Marjolein Dijkstra. A boltzmann generator for the isobaric-isothermal ensemble. *arXiv preprint arXiv:2305.08483*, 2023.
- Francisco Vargas, Will Grathwohl, and Arnaud Doucet. Denoising diffusion samplers. *arXiv preprint arXiv:2302.13834*, 2023.
- Hao Wu, Jonas Köhler, and Frank Noé. Stochastic normalizing flows. *Advances in Neural Information Processing Systems*, 33:5933–5944, 2020.
- Qinsheng Zhang and Yongxin Chen. Path integral sampler: a stochastic control approach for sampling. *arXiv preprint arXiv:2111.15141*, 2021.
- Yichuan Zhang and José Miguel Hernández-Lobato. Ergodic inference: Accelerate convergence by optimisation. *arXiv preprint arXiv:1805.10377*, 2018.
- Shuxin Zheng, Jiyan He, Chang Liu, Yu Shi, Ziheng Lu, Weitao Feng, Fusong Ju, Jiayi Wang, Jianwei Zhu, Yaosen Min, et al. Towards predicting equilibrium distributions for molecular systems with deep learning. *arXiv preprint arXiv:2306.05445*, 2023.

A PROOF OF (5)

For an extremely small lag time τ , the Euler-Maruyama discretization of $z_{[\cdot]}$ in the decoding process provides

$$z_t = z_{t-\tau} + f(z_{t-\tau}, t - \tau)\tau + \sqrt{\tau}g(t-\tau)u_{t-\tau}, \quad (10)$$

$$z_{t-\tau} = z_t - (f(z_t, t) - g(t)^2\nabla \log p_D(z_t))\tau + \sqrt{\tau}g(t)\bar{u}_t, \quad (11)$$

where $u_{t-\tau}, \bar{u}_t \sim \mathcal{N}(\cdot|0, I)$. Importantly, $u_{t-\tau}$ is independent of $\{z_{t'}|t' \leq t - \tau\}$ and x , and \bar{u}_t is independent of $\{z_{t'}|t' \geq t\}$. The Euler-Maruyama approximation of $p_E(z_{[\cdot]}|x)$ gives

$$z_{t-\tau} = z_t - (f(z_t, t) - g(t)^2s(z_t, x, t))\tau + \sqrt{\tau}g(t)v_t \quad (12)$$

with $v_t \sim \mathcal{N}(\cdot|0, I)$.

According to (11, 12), we can obtain

$$\begin{aligned} \mathbb{E}_{p_D} [\log p_D(z_{t-\tau}|z_t)] &= -\frac{d}{2} \log 2\pi - \frac{d}{2} \log \tau g(t)^2 \\ &\quad - \frac{1}{2} \tau^{-1} g(t)^{-2} \mathbb{E}_{p_D} \left[\left\| z_{t-\tau} - z_t + (f(z_t, t) - g(t)^2 \nabla \log p_D(z_t)) \tau \right\|^2 \right] \\ &= -\frac{d}{2} \log 2\pi - \frac{d}{2} \log \tau g(t)^2 - \frac{1}{2} \tau^{-1} g(t)^{-2} \mathbb{E}_{p_D} \left[\left\| \sqrt{\tau} g(t) \bar{u}_t \right\|^2 \right] \\ &= -\frac{d}{2} \log 2\pi - \frac{d}{2} \log \tau g(t)^2 - \frac{d}{2} \end{aligned} \quad (13)$$

and

$$\begin{aligned} \mathbb{E}_{p_D} [\log p_E(z_{t-\tau}|z_t, x)] &= -\frac{d}{2} \log 2\pi - \frac{d}{2} \log \tau g(t)^2 \\ &\quad - \frac{1}{2} \tau^{-1} g(t)^{-2} \mathbb{E}_{p_D} \left[\left\| z_{t-\tau} - z_t + (f(z_t, t) - g(t)^2 s(z_t, x)) \tau \right\|^2 \right] \\ &= -\frac{d}{2} \log 2\pi - \frac{d}{2} \log \tau g(t)^2 \\ &\quad - \frac{1}{2} \tau^{-1} g(t)^{-2} \mathbb{E}_{p_D} \left[\left\| z_{t-\tau} - z_t + f(z_t, t) \tau \right\|^2 \right] \\ &\quad - \frac{1}{2} \tau^{-1} g(t)^{-2} \mathbb{E}_{p_D} \left[\left\| g(t)^2 s(z_t, x) \tau \right\|^2 \right] \\ &\quad + \tau^{-1} g(t)^{-2} \mathbb{E}_{p_D} \left[(z_{t-\tau} - z_t + f(z_t, t) \tau)^\top g(t)^2 s(z_t, x) \tau \right] \\ &= -\frac{d}{2} \log 2\pi - \frac{d}{2} \log \tau g(t)^2 \\ &\quad - \frac{1}{2} \tau^{-1} g(t)^{-2} \mathbb{E}_{p_D} \left[\left\| g(t)^2 \nabla \log p_D(z_t) \tau + \sqrt{\tau} g(t) \bar{u}_t \right\|^2 \right] \\ &\quad - \frac{1}{2} \tau g(t)^2 \mathbb{E}_{p_D} \left[\left\| s(z_t, x) \right\|^2 \right] \\ &\quad + \mathbb{E}_{p_D} \left[(z_{t-\tau} - z_t + f(z_t, t) \tau)^\top s(z_t, x) \right] \\ &\stackrel{(i)}{=} -\frac{d}{2} \log 2\pi - \frac{d}{2} \log \tau g(t)^2 - \frac{d}{2} \\ &\quad - \frac{1}{2} \tau g(t)^2 \mathbb{E}_{p_D} \left[\left\| \nabla \log p_D(z_t) \right\|^2 \right] \\ &\quad - \frac{1}{2} \tau g(t)^2 \mathbb{E}_{p_D} \left[\left\| s(z_t, x) \right\|^2 \right] \\ &\quad + \mathbb{E}_{p_D} \left[(z_{t-\tau} - z_t + f(z_t, t) \tau)^\top s(z_t, x) \right], \end{aligned} \quad (14)$$

where (i) results from the independence between \bar{u}_t and z_t .

By using (10) and the first-order Taylor expansion, we have

$$\begin{aligned}
z_{t-\tau} - z_t + f(z_t, t)\tau &= z_{t-\tau} - (z_{t-\tau} + f(z_{t-\tau}, t - \tau)\tau + \sqrt{\tau}g(t - \tau)u_{t-\tau}) \\
&\quad + f(z_{t-\tau} + f(z_{t-\tau}, t)\tau + \sqrt{\tau}g(t - \tau)u_{t-\tau}, t)\tau \\
&= -f(z_{t-\tau}, t - \tau)\tau - \sqrt{\tau}g(t - \tau)u_{t-\tau} \\
&\quad + \tau f(z_{t-\tau}, t - \tau) \\
&\quad + \tau \frac{\partial f(z_{t-\tau}, t - \tau)}{\partial z_{t-\tau}} (z_t - z_{t-\tau}) \\
&\quad + \tau^2 \frac{\partial f(z_{t-\tau}, t - \tau)}{\partial t} \\
&\quad + \tau \cdot O\left(\|z_t - z_{t-\tau}\|^2 + \tau^2\right) \\
&= -\sqrt{\tau}g(t - \tau)u_{t-\tau} \\
&\quad + \tau \frac{\partial f(z_{t-\tau}, t - \tau)}{\partial z_{t-\tau}} (f(z_{t-\tau}, t - \tau)\tau + \sqrt{\tau}g(t - \tau)u_{t-\tau}) \\
&\quad + \tau^2 \frac{\partial f(z_{t-\tau}, t - \tau)}{\partial t} \\
&\quad + \tau \cdot O\left(\|f(z_{t-\tau}, t - \tau)\tau + \sqrt{\tau}g(t - \tau)u_{t-\tau}\|^2 + \tau^2\right) \\
&= -\sqrt{\tau}g(t - \tau)u_{t-\tau} + O(\tau^2)
\end{aligned}$$

and

$$\begin{aligned}
s(z_t, x, t) &= s(z_{t-\tau}, x, t - \tau) + \frac{\partial s(z_{t-\tau}, x, t - \tau)}{\partial z_{t-\tau}} (z_t - z_{t-\tau}) + \frac{\partial s(z_{t-\tau}, x, t - \tau)}{\partial t} \tau \\
&= s(z_{t-\tau}, x, t - \tau) \\
&\quad + \frac{\partial s(z_{t-\tau}, x, t - \tau)}{\partial z_{t-\tau}} (f(z_{t-\tau}, t - \tau)\tau + \sqrt{\tau}g(t - \tau)u_{t-\tau}) \\
&\quad + \frac{\partial s(z_{t-\tau}, x, t - \tau)}{\partial t} \tau \\
&= s(z_{t-\tau}, x, t - \tau) + \sqrt{\tau} \frac{\partial s(z_{t-\tau}, x, t - \tau)}{\partial z_{t-\tau}} g(t - \tau)u_{t-\tau} + O(\tau).
\end{aligned}$$

Combining the two equations above, we get

$$\begin{aligned}
\mathbb{E}_{p_D} \left[(z_{t-\tau} - z_t + f(z_t, t)\tau)^\top s(z_t, x, t) \right] &= \mathbb{E}_{p_D} \left[-\sqrt{\tau}g(t - \tau)u_{t-\tau}^\top s(z_{t-\tau}, x, t - \tau) \right] \\
&\quad - \tau g(t - \tau)^2 \mathbb{E}_{p_D} \left[u_{t-\tau}^\top \frac{\partial s(z_{t-\tau}, x, t - \tau)}{\partial z_{t-\tau}} u_{t-\tau} \right] \\
&\quad + o(\tau) \\
&\stackrel{(ii)}{=} -\tau g(t - \tau)^2 \mathbb{E}_{p_D} \left[\text{tr} \left(\frac{\partial s(z_{t-\tau}, x, t - \tau)}{\partial z_{t-\tau}} \right) \right] \\
&\quad + o(\tau), \tag{15}
\end{aligned}$$

where (ii) follows from the fact that $u_{t-\tau}$ is independent of $z_{t-\tau}$ and x in the decoding process. Taking into account (15), (13) and (14), we arrive at the following results:

$$\begin{aligned}
\Delta_t &\triangleq \mathbb{E}_{p_D} [\log p_D(z_{t-\tau}|z_t)] - \mathbb{E}_{p_D} [\log p_E(z_{t-\tau}|z_t, x)] \\
&= \frac{1}{2} \tau g(t)^2 \mathbb{E}_{p_D} \left[\|\nabla \log p_D(z_t)\|^2 \right] \\
&\quad + \frac{1}{2} \tau g(t)^2 \mathbb{E}_{p_D} \left[\|s(z_t, x, t)\|^2 \right] \\
&\quad + \tau g(t - \tau)^2 \mathbb{E}_{p_D} \left[\text{tr} \left(\frac{\partial s(z_{t-\tau}, x, t - \tau)}{\partial z_{t-\tau}} \right) \right] + o(\tau).
\end{aligned}$$

Let $\tau = T/L$, where L is a large number, we have

$$\begin{aligned} \mathbb{E}_{p_D} \left[\log \frac{p_D(x, z_0, z_\tau, \dots, z_T)}{p_E(x, z_0, z_\tau, \dots, z_T)} \right] &= \mathbb{E}_{p_D} \left[\log \frac{p_D(x|z_0)p_D(z_T) \prod_{l=1}^L p_D(z_{(l-1)\tau}|z_{l\tau})}{\pi(x)p_E(z_T) \prod_{l=1}^L p_E(z_{(l-1)\tau}|z_{l\tau}, x)} \right] \\ &= \mathbb{E}_{p_D} \left[\log \frac{p_D(x|z_0)}{Z^{-1} \exp(-U(x))} \right] + \sum_{l=1}^L \Delta_{l\tau} \\ &= \mathbb{E}_{p_D} [\log p_D(x|z_0) + U(x)] + \log Z + \sum_{l=1}^L \Delta_{l\tau} \end{aligned}$$

and

$$\begin{aligned} \mathbb{E}_{p_D} \left[\log \frac{p_D(x, z_{[\cdot]})}{p_E(x, z_{[\cdot]})} \right] &= \lim_{L \rightarrow \infty} \mathbb{E}_{p_D} \left[\log \frac{p_D(x, z_0, z_\tau, \dots, z_T)}{p_E(x, z_0, z_\tau, \dots, z_T)} \right] \\ &= \mathbb{E}_{p_D} [\log p_D(x|z_0) + U(x)] \\ &\quad + \int \frac{g(t)^2}{2} \mathbb{E}_{p_D} \left[\|s(z_t, x, t)\|^2 + 2\text{tr} \left(\frac{\partial s(z_t, x, t)}{\partial z_t} \right) + \|\nabla \log p_D(z_t)\|^2 \right] dt \\ &\quad + \log Z. \end{aligned}$$

B NORMALIZING CONSTANT APPROXIMATION AND IMPORTANCE SAMPLING VIA MARGINAL ENCODER DENSITY

Eq. (1) provides a lower bound for $\log Z$ as follows:

$$\log Z \geq -\mathbb{E}_{p_D(x, z_0|\phi)} \left[\log \frac{p_D(z_0)p_D(x|z_0, \phi)}{p_E(z_0|x, \theta)} + U(x) \right].$$

The tightness of this bound is achieved when $p_D(x, z_0|\phi)$ closely approximates $p_E(x, z_0|\theta) = \pi(x) \cdot p_E(z_0|x, \theta)$. Based on (9), we can employ an ODE solver to efficiently compute $p_E(z_0|x, \theta)$, thereby enabling the calculation of a variational approximation for $\log Z$.

Furthermore, leveraging the value of $p_E(z_0|x, \theta)$ obtained from the ODE solver, we can unbiasedly estimate the value of $\mathbb{E}\pi[O(x)]$ through importance sampling. Let x^1, \dots, x^N represent N samples generated by the decoder in EDG with latent variables $z_0^1, \dots, z_0^N \sim \mathcal{N}(0, I)$. The estimation is given by:

$$\begin{aligned} \mathbb{E}_{\pi(x)}[O(x)] &= \mathbb{E}_{p_D(z_0)p_D(x|z_0)} \left[O(x) \frac{\pi(x)p_E(z_0|x)}{p_D(z_0)p_D(x|z_0)} \right], \\ &\approx \frac{1}{N} \sum_n O(x^n) \frac{\pi(x^n)p_E(z_0^n|x^n)}{p_D(z_0^n)p_D(x^n|z_0^n)}. \end{aligned}$$

C IMPORTANCE WEIGHTING FOR ACCURATE TIME INTEGRAL

It can be seen from (7) that an ideal choice for the time proposal $p(t)$ in Monte Carlo estimation of the integral on the right-hand side is given by

$$p(t) \propto g(t)^2 \mathbb{E}_{p(\epsilon)p_D(x, z_t)} [\mathcal{L}_t(x, z_t, \epsilon; \theta)].$$

In our experiments, we approximate the ideal proposal using the strategy introduced in (Choi et al., 2022). The implementation details are as follows: We maintain a history buffer containing values of \mathcal{L}_t from the most recent $B_{\text{buffer}} = 30$ minibatches. In each iteration, the buffer provides an estimate of the expected value of \mathcal{L}_t as a function of t using a histogram with $K_{\text{bin}} = 100$ bins over the time interval $[0, T]$. Subsequently, we obtain an estimate of the ideal $p(t)$ for each iteration. Initially, during the early stages of training, $p(t)$ is set as a uniform distribution until B_{buffer} minibatches are accumulated.

D EXPERIMENTAL DETAILS

EDG In our experiments, we leverage the subVP SDE proposed in (Song et al., 2020) to model the diffusion process of z_t in (2), defined as

$$dz_t = -\frac{1}{2}\beta(t)z_t dt + \sqrt{\beta(t)\left(1 - e^{-2\int_0^t \beta(s)ds}\right)} dW_t$$

with $T = 1$. Here, $\beta(t) = \beta_{\min} + t(\beta_{\max} - \beta_{\min})$, and we set $\beta_{\min} = 0.1$ and $\beta_{\max} = 20$ for experiments. The initial state z_0 follows a standard Gaussian distribution. Line 1 of Algorithm 1 is implemented as

$$y := \mu_0(\zeta_0; \phi) + \Sigma_0(\zeta_0; \phi)\zeta_1,$$

where $\zeta = (\zeta_0, \zeta_1)$, and $\mu_0(\zeta_0; \phi), \Sigma_0(\zeta_0; \phi)$ are modeled by MLPs. When incorporating the GHD in the decoder, we set $K = 10$ and $J = 5$. However, in the absence of GHD, denoted as "EDG w/o GHD" in Section 4, we set $K = J = 0$, and Lines 2-8 of Algorithm 1 are not implemented. Our numerical experience suggests that, for EDG without GHD based decoder, this particular setting outperforms the direct use of MLPs to model $\mu(z_0; \phi), \Sigma(z_0; \phi)$.

Baseline In order to illustrate the superiority of our model, we compare EDG with long mixing time HMC, VAE with trainable Gauss Encoder (e.g. $p_E(z|x) = \mathcal{N}(z; \mu_\theta(x), \Sigma_\theta(x))$) and Boltzmann generator (BG) with RealNVP (Dinh et al., 2016). For the VAE, it initiates from a high-dimensional latent variable $z_0 \in R^{30}$, comprising a three-layer fully connected network, each encompassing 256 units, interconnected using the ReLU activation function. Regarding the BG, we construct it using a three-layer fully connected structure of the RealNVP, provided with 256 units for each layer and associated with the ReLU activation function.

2D energy function We use the following model architectures to generate samples for 2D energy tasks. 'fc n ' denotes a fully connected layer with n neurons.

The model architecture of 2D energy tasks	
Decoding process	Encoding process
Network gauss:	Score network:
fc 2×32 , ReLU, $2 \times (\text{fc } 32 \times 32, \text{ ReLU})$, fc 32×2 .	fc 25×16 , ReLU,
if GHD:	fc 16×16 , ReLU,
Q_v, T_v :	fc 16×22 .
fc 5×10 , Tanh, fc 10×10 , Tanh, fc 10×2 .	
Q_x, T_x :	
fc 3×10 , ReLU, fc 10×10 , ReLU, fc 10×2 .	
Langevin network:	
fc 2×10 , ReLU, fc 10×10 , ReLU, fc 10×2 .	

Reference samples for Mog2, Mog2(i), Mog6, and Mog9 in Fig. 2 are precisely drawn from the target distributions, as these distributions are mixtures of Gaussian distributions. Reference samples for Ring and Ring5 are generated using the Metropolis-Hastings algorithm, with Gaussian distributions of variances 9 and 25, respectively, serving as proposal distributions. For the HMC, we employ the use of an HMC run of a total length of 2,000 steps, initiating from a standard normal distribution. The first 1,000 steps are designated as burn-in steps followed by a subsequent 1,000 steps used for sample generation. This procedure is independently executed 500 times for the purpose of creating the visual representation.

Given the reference samples $X = \{x_i\}_{i=1}^m$ and the generated samples $Y = \{y_i\}_{i=1}^m$, the Maximum Mean Discrepancy (MMD) (Gretton et al., 2012) measures the difference between the distributions of X and Y as follows:

$$\text{MMD}^2(X, Y) = \frac{1}{m(m-1)} \sum_i \sum_{j \neq i} k(x_i, x_j) - \frac{2}{m^2} \sum_i \sum_j k(x_i, y_j) + \frac{1}{m(m-1)} \sum_i \sum_{j \neq i} k(y_i, y_j)$$

where $k(\cdot, \cdot)$ denotes the kernel function to compute the inner product. RBF kernel is used in Table 1, and the bandwidth is set as the median distance between corresponding samples. We execute 10 cycles for each model to procure 5,000 desired samples, following which we evaluate the mean and standard deviation of Maximum Mean Discrepancy (MMD) in relation to 5,000 reference data.

Bayesian Logistic Regression In all experiments, we employ the same data partition and the datasets are divided into training and test sets at a ratio of 4:1. Before training, we normalize all datasets to have zero mean and unit variance. For d -dimensional features, the architectures of neural networks involved in the EDG are as follows:

The model architecture of Bayesian Logistic Regression	
Decoding process	Encoding process
Network gauss: fc $d \times 256$, ReLU, $2 \times (\text{fc } 256 \times 256, \text{ReLU})$, fc 256×256 .	Score network: fc $(12d + 1) \times 256$, ReLU,
if GHD: Q_v, T_v : fc $(2d + 1) \times 256$, Tanh, fc 256×256 , Tanh, fc $256 \times d$.	fc 256×256 , ReLU, fc $256 \times 11d$.
Q_x, T_x : fc $(d + 1) \times 256$, ReLU, fc 256×256 , ReLU, fc $256 \times d$.	
Langevin network: fc $11d \times 256$, ReLU, fc 256×256 , ReLU, fc $256 \times d$.	

In the task of covertype, $x = (\alpha, w, b)$ with the prior distribution $p(x) = p(\alpha)p(w, b|\alpha)$, where $p(\alpha) = \text{Gamma}(\alpha; 1, 0.01)$ and $p(w, b|\alpha) = \mathcal{N}(w, b; 0, \alpha^{-1})$.